Acta Crystallographica Section B
Structural Science
ISSN 0108-7681

Structures of $K_{0.05}Na_{0.95}NbO_3$ (50–300 K) and $K_{0.30}Na_{0.70}NbO_3$ (100–200 K)

N. Zhang,[a]* A. M. Glazer,[a] D. Baker[b] and P. A. Thomas[b]

[a]Department of Physics, University of Oxford, Parks Road, Oxford OX1 3PU, England, and [b]Department of Physics, University of Warwick, Coventry CV4 7AL, England

Correspondence e-mail: n.zhang1@physics.ox.ac.uk

Received 13 December 2008
Accepted 25 March 2009

Rietveld refinement using neutron powder diffraction data is reported for the potential lead-free piezoelectric material $K_xNa_{1-x}NbO_3$ (x = 0.05, x = 0.3) at low temperatures. The structures were determined to be of rhombohedral symmetry, space group $R3c$, with the tilt system $a^-a^-a^-$ for both compositions. It was found that some of the structural parameters differ significantly in the two structures, and particularly the NbO_6 octahedral strains as a function of temperature. The 300 K profile for $K_{0.05}Na_{0.95}NbO_3$ shows the coexistence of rhombohedral and monoclinic phases, which indicates that the phase boundary is close to room temperature; the phase boundary for $K_{0.30}Na_{0.70}NbO_3$ is found to be at approximately 180 K.

1. Introduction

Solid solutions of $K_xNa_{1-x}NbO_3$ (KNN) have been widely studied because they are promising candidates as lead-free piezoelectric materials for replacing PZT ($PbZr_{1-x}Ti_xO_3$), which contains the environmentally harmful element lead (Pb). The original phase diagram of KNN at room temperature and above was reported by Ahtee & Glazer (1976). In the phase diagram, three phase boundaries at room temperature were indicated at around $x \simeq 0.50$, $x \simeq 0.32$ and $x \simeq 0.18$. The $x \simeq 0.50$ phase boundary has been discussed most widely because of the suggestion of it being a morphotropic phase boundary (MPB; Saito *et al.*, 2004), which, by analogy with PZT (Glazer *et al.*, 2004), might be considered to be a potential area of maximum piezoelectric behavior. Structural studies of $K_xNa_{1-x}NbO_3$ (x = 0.02, 0.1, 0.2, 0.35) have been reported by Ahtee & Hewat (1975, 1978); the room- and high-temperature behaviours of $K_xNa_{1-x}NbO_3$ (x = 0.3) have been published by Baker *et al.* (2009*a*).

However, the low-temperature phases of KNN have been studied relatively little up until now. Some studies on the sodium niobate end-member have been published by Darlington & Megaw (1973) and Mishra *et al.* (2007), showing that at low temperature it undergoes an antiferroelectric ferroelectric phase transition from orthorhombic $Pbcm$ to rhombohedral $R3c$. However, the potassium niobate end-member is rhombohedral, $R3m$, below 263 K (Hewat, 1973). The purpose of this paper is to give a definitive view of sodium-rich $K_xNa_{1-x}NbO_3$ at low temperatures and also to determine the phase boundaries between the low- and room-temperature phases. Owing to the possible phase boundary around $x = 0.3$ and the structural complexity at the sodium-rich end, the $x = 0.30$ and $x = 0.05$ samples were chosen for this investigation.

2. Specimen preparation and experimental details

Na_2CO_3, K_2CO_3 and Nb_2O_5 powders were ground using a ball-milling machine for 10 h, and then calcined at 1223 K for 12 h. Subsequently, the specimens were removed, ground again and sintered at 1323 K for 24 h. The ratio of sodium and potassium of the first sample ($K_{0.05}Na_{0.95}NbO_3$) was examined by Jeol JSM-840A scanning electron microscopy. The mass concentration of the atoms was measured using the ZAF correction method and the fractions of each element were calculated. The sodium percentage was found to be 5.0 ± 0.3%. The second sample ($K_{0.30}Na_{0.70}NbO_3$) was checked using variable-pressure energy-dispersive X-ray analysis (EDX) on a Zeiss Supra 55VP FEG SEM (scanning electron microscope) with EDAX *Genesis* software, and the sodium percentage was 32 ± 2%.

Neutron powder diffraction data were collected using the high-resolution two-axis diffractometer (D2B) at the ILL, Grenoble, at room temperature and at low temperatures. The wavelength used was 1.60 Å. The data were collected over the range $0.10 < 2\theta < 159.9°$, in 0.05° steps. For low-temperature measurements, a standard Orange Cryostat available at ILL was used.

The $K_{0.05}Na_{0.95}NbO_3$ data were collected from 50 to 300 K in steps of 50 K. The $K_{0.30}Na_{0.70}NbO_3$ sample was heated from 100 K and the diffraction pattern was checked every 20 K with increasing temperature until a change in the pattern appeared at ∼ 200 K. All the neutron data were refined by the Rietveld

Table 1
Fractional coordinates for the hexagonal setting of rhombohedral perovskites, space group *R*3*c*.

Atom type	*x*/*a*	*y*/*b*	*z*/*c*
Na/K	0	0	$1/4 + s$
Nb	0	0	t
O	$1/6 - 2e - 2d$	$1/3 - 4d$	1/12

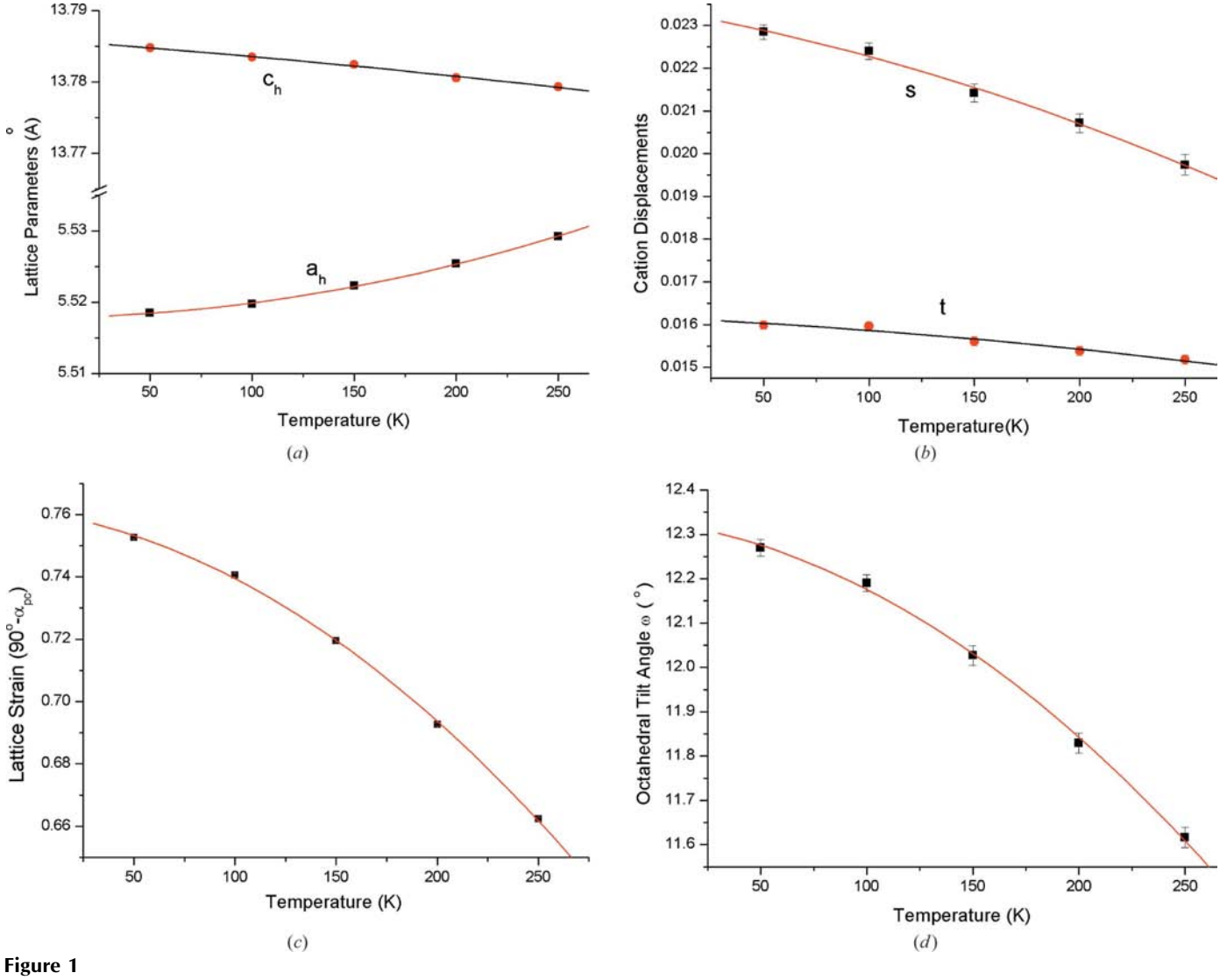

Figure 1
Structural parameters of $Na_{0.95}K_{0.05}NbO_3$ as a function of temperature in the rhombohedral phase: (*a*) lattice parameters; (*b*) cation displacements (in coordinates); (*c*) lattice strain ($90 - \alpha_{pc}$); (*d*) tilt angle ω.

Table 2
Experimental details and refinement results for $Na_{0.95}K_{0.05}NbO_3$ at low temperatures.

The strain parameter ζ and the angle $(90 - \alpha)$ are calculated from the unit-cell parameters, and the tilt angle ω is calculated from the parameter e.

	50 K	100 K	150 K	200 K	250 K
Crystal data					
Chemical formula	$K_{0.05}Na_{0.95}NbO_3$	$K_{0.05}Na_{0.95}NbO_3$	$K_{0.05}Na_{0.95}NbO_3$	$K_{0.05}Na_{0.95}NbO_3$	$K_{0.05}Na_{0.95}NbO_3$
M_r	164.71	164.71	164.71	164.71	164.71
Crystal system, space group	Trigonal, *R*3*c*	Trigonal, *R*3*c*	Trigonal, *R*3*c*	Trigonal, *R*3*c*	Trigonal, *R*3*c*
a, *c* (Å)	5.51848 (4), 13.7848 (2)	5.51972 (4), 13.7835 (2)	5.52229 (5), 13.7824 (2)	5.52539 (5), 13.7806 (2)	5.52922 (5), 13.7793 (2)
V (Å^3)	363.55 (1)	363.68 (1)	363.99 (1)	364.35 (1)	364.83 (1)
Z	6	6	6	6	6
Radiation type	Neutron	Neutron	Neutron	Neutron	Neutron
Wavelength of incident radiation (Å)	1.60	1.60	1.60	1.60	1.60
Specimen shape, size (mm)	Cylinder, 20 × 50 × 20	Cylinder, 20 × 50 × 20	Cylinder, 20 × 50 × 20	Cylinder, 20 × 50 × 20	Cylinder, 20 × 50 × 20
Data collection					
Diffractometer	D2B	D2B	D2B	D2B	D2B
Specimen mounting	Vanadium can packed with powder	Vanadium can packed with powder	Vanadium can packed with powder	Vanadium can packed with powder	Vanadium can packed with powder
Scan method	Step	Step	Step	Step	Step
Data-collection mode	Reflection	Reflection	Reflection	Reflection	Reflection
2θ values (°)	$2\theta_{min}$ = 0.10, $2\theta_{max}$ = 160, $2\theta_{step}$ = 0.05	$2\theta_{min}$ = 0.10, $2\theta_{max}$ = 160, $2\theta_{step}$ = 0.05	$2\theta_{min}$ = 0.10, $2\theta_{max}$ = 160, $2\theta_{step}$ = 0.05	$2\theta_{min}$ = 0.10, $2\theta_{max}$ = 160, $2\theta_{step}$ = 0.05	$2\theta_{min}$ = 0.10, $2\theta_{max}$ = 160, $2\theta_{step}$ = 0.05
Refinement					
R_p, R_{wp}, R_{exp}, χ^2	0.050, 0.066, 0.017, 3.84	0.050, 0.067, 0.018, 3.50	0.053, 0.070, 0.019, 3.61	0.053, 0.069, 0.019, 3.61	0.050, 0.067, 0.018, 3.65
Excluded region(s)	145–160	145–160	145–160	145–160	145–160
Profile function	Chebychev with six coefficients	Chebychev with six coefficients	Chebychev with six coefficients	Chebychev with six coefficients	Chebychev with six coefficients
No. of data points	2601	2601	2601	2601	2601
No. of parameters	24	24	24	24	24
No. of restraints	None	None	None	None	None
s	0.0229 (2)	0.0224 (2)	0.0214 (2)	0.0207 (2)	0.0197 (2)
t	0.0160 (1)	0.0160 (1)	0.0156 (1)	0.0154 (1)	0.0152 (1)
d	−0.00083 (8)	−0.00090 (8)	−0.00079 (9)	−0.00083 (9)	−0.00091 (0)
e	0.03139 (5)	0.03118 (5)	0.03075 (6)	0.03023 (6)	0.02967 (6)
ω (°)	12.27 (2)	12.19 (2)	12.03 (2)	11.83 (2)	11.62 (2)
$\zeta \times 10^2$	−0.352 (7)	−0.353 (7)	−0.347 (9)	−0.343 (8)	−0.345 (8)
$90 - \alpha_{pc}$ (°)	0.7527 (5)	0.7406 (5)	0.7196 (6)	0.6927 (6)	0.6623 (6)
$BV_{Na/K-O}$	1.05	1.04	1.03	1.02	1.01
BV_{Nb-O}	4.67	4.66	4.67	4.67	4.67

method using the software *TOPAS Academic* (Coelho, 2005). Bond valences (BV) were calculated for each structure to check that the models refined were reasonable. The bond valences were calculated from the bond lengths according to Brown's (1981) theory. Effective BV for the *A*-site atoms were calculated according to their refined occupancies.

3. Low-temperature phases

3.1. $K_{0.05}Na_{0.95}NbO_3$ for $50 \leq T \leq 250$ K

At 250 K or below, the data were refined in the rhombohedral *R*3*c* space group assuming anti-phase tilting of the oxygen octahedra $a^-a^-a^-$, using Glazer's (1972) notation. Hexagonal axes (a_H and c_H) were chosen for the refinement, thus allowing several important structural parameters, highlighted for rhombohedral perovskites by Megaw & Darlington (1975), to be refined separately according to the fractional coordinates shown in Table 1.

Both isotropic and anisotropic displacement parameters were refined. In the anisotropic case, because of the low temperature, most of the parameters (U^{ij}) were close to zero with large errors. In general, use of isotropic displacement parameters was more successful, although values were frequently less than zero. An absorption correction was tried using the suggestion of Hewat (1979), in which the correction for the Debye–Waller factor can be expressed by the formula

$$\Delta B = \lambda^2[b_1\mu r + b_2(\mu r)^2], \quad (1)$$

where b_1 and b_2 are constants, and $\lambda = 1.60$ Å for diffractometer D2B. For $K_{0.05}Na_{0.95}NbO_3$ at 50 K, the lowest B_{iso} was −0.13 Å^2. If $\mu r \geq 0.33$, which is in the reasonable range for niobium absorption on the D2B instrument, B_{iso} is then corrected by (1) to be above zero. The same correction was

also applied to the low-temperature models for $K_{0.30}Na_{0.70}NbO_3$.

All the structural parameters were calculated from the refinement results using the geometrical relationships for rhombohedral *R*3*c* perovskites. Bond-valence calculations suggested that the Nb atoms are slightly under-bonded, whilst the Na/K valences are close to 1. The parameters at different temperatures are compared in Table 2.

As discussed by Megaw & Darlington (1975), the parameter *s* describes fractional displacements of the *A* cations along c_H ($[111]_p$ direction of the pseudocubic cell) from the ideal perovskite structure site, and *t* measures the shift of the B cations along the same direction from the centre of the octahedron. Na and K positions were fixed to have a single *s* parameter. The cation shifts are plotted against temperature and a gradual decrease can be observed (Fig. 1*b*), which is consistent with the trend of the phase change from rhombohedral *R*3*c* to monoclinic *Pm*.

The rhombohedral angle, α_{pc}, in the pseudocubic cell is derived from the lattice parameters of the hexagonal cell a_H and c_H [$\cos\alpha_{pc} = (c_H^2 - 6a_H^2)/(c_H^2 + 12a_H^2)$]. The lattice strain, which is defined by the deviation of the rhombohedral angle from 90°, is plotted as a function of temperature in Fig. 1(*c*). The rhombohedral angle is less than 90°, which is consistent with the general behaviour of rhombohedral ferroelectric perovskites (Thomas, 1996). As the temperature increases up to 300 K, the α_{pc} value increases by $\sim 0.1°$, but does not reach 90°.

The parameter *e* indicates the rotation of an octahedron face about the triad axis, and this leads to the tilt angle ω *via* $\tan\omega = 4(3)^{1/2}e$. Fig. 1(*d*) shows a plot of ω from 50 to 250 K. A gradual decrease is observed as the temperature rises towards the phase boundary.

The parameter *d* describes the octahedral distortion, keeping triad-axis symmetry, but making the size of the upper and lower faces different. *d* is negative for $K_{0.05}Na_{0.95}NbO_3$

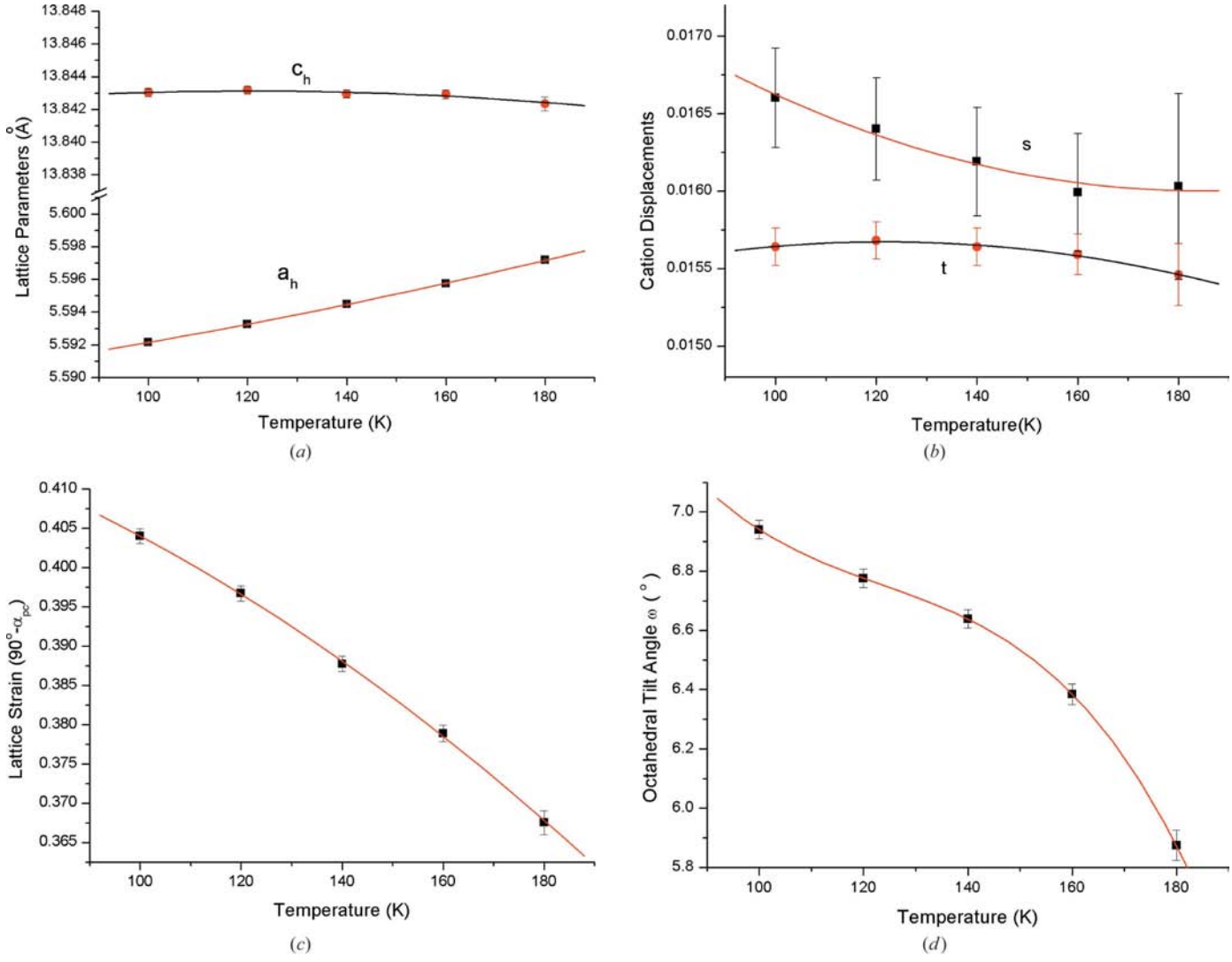

Figure 2
Structural parameters of $Na_{0.70}K_{0.30}NbO_3$ as a function of temperature in the rhombohedral phase: (*a*) lattice parameters; (*b*) cation displacements (in coordinates); (*c*) lattice strain ($90 - \alpha_{pc}$); (*d*) tilt angle ω.

Table 3
Experimental details and refinement results for $Na_{0.70}K_{0.30}NbO_3$ at low temperatures.

The strain parameter ζ and the angle $(90 - \alpha)$ are calculated from the unit-cell parameters, and the tilt angle ω is calculated from the parameter e.

	100 K	120 K	140 K	160 K	180 K
Crystal data					
Chemical formula	$K_{0.30}Na_{0.70}NbO_3$	$K_{0.30}Na_{0.70}NbO_3$	$K_{0.30}Na_{0.70}NbO_3$	$K_{0.30}Na_{0.70}NbO_3$	$K_{0.30}Na_{0.70}NbO_3$
M_r	168.73	168.73	168.73	168.73	168.73
Crystal system, space group	Trigonal, *R*3*c*	Trigonal, *R*3*c*	Trigonal, *R*3*c*	Trigonal, *R*3*c*	Trigonal, *R*3*c*
a, *c* (Å)	5.59214 (6), 13.8430 (2)	5.59326 (6), 13.8432 (2)	5.59447 (6), 13.8429 (3)	5.59575 (6), 13.8429 (3)	5.5972 (1), 13.8423 (4)
V (Å^3)	374.90 (1)	375.06 (1)	375.21 (1)	375.38 (1)	375.56 (2)
Z	6	6	6	6	6
Radiation type	Neutron	Neutron	Neutron	Neutron	Neutron
Wavelength of incident radiation (Å)	1.60	1.60	1.60	1.60	1.60
Specimen shape, size	Cylinder, 20 × 50 × 20	Cylinder, 20 × 50 × 20	Cylinder, 20 × 50 × 20	Cylinder, 20 × 50 × 20	Cylinder, 20 × 50 × 20
Data collection					
Diffractometer	D2B	D2B	D2B	D2B	D2B
Specimen mounting	Vanadium can packed with powder	Vanadium can packed with powder	Vanadium can packed with powder	Vanadium can packed with powder	Vanadium can packed with powder
Scan method	Step	Step	Step	Step	Step
Data-collection mode	Reflection	Reflection	Reflection	Reflection	Reflection
2θ values (°)	$2\theta_{min}$ = 0.10, $2\theta_{max}$ = 160, $2\theta_{step}$ = 0.05	$2\theta_{min}$ = 0.10, $2\theta_{max}$ = 160, $2\theta_{step}$ = 0.05	$2\theta_{min}$ = 0.10, $2\theta_{max}$ = 160, $2\theta_{step}$ = 0.05	$2\theta_{min}$ = 0.10, $2\theta_{max}$ = 160, $2\theta_{step}$ = 0.05	$2\theta_{min}$ = 0.10, $2\theta_{max}$ = 160, $2\theta_{step}$ = 0.05
Refinement					
R_p, R_{wp}, R_{exp}, χ^2	0.055, 0.075, 0.027, 2.72	0.055, 0.075, 0.027, 2.72	0.056, 0.076, 0.027, 2.80	0.059, 0.079, 0.027, 2.89	0.085, 0.114, 0.027, 4.20
Excluded regions	145–160	145–160	145–160	145–160	145–160
Profile function	Chebychev with six coefficients	Chebychev with six coefficients	Chebychev with six coefficients	Chebychev with six coefficients	Chebychev with six coefficients
No. of data points	2601	2601	2601	2601	2601
No. of parameters	24	24	24	24	24
No. of restraints	None	None	None	None	None
s	0.0166 (3)	0.0164 (3)	0.0162 (4)	0.0160 (4)	0.0160 (6)
t	0.0156 (1)	0.0157 (1)	0.0156 (1)	0.0156 (1)	0.0155 (2)
d	−0.0007 (1)	−0.0007 (1)	−0.0007 (1)	−0.0008 (1)	−0.0009 (2)
e	0.01757 (7)	0.01715 (7)	0.01680 (7)	0.01615 (7)	0.0149 (1)
ω (°)	6.94 (3)	6.78 (3)	6.64 (3)	6.38 (3)	5.87 (4)
$\zeta \times 10^2$	0.322 (7)	0.333 (7)	0.340 (7)	0.363 (7)	0.42 (1)
$90 - \alpha_{pc}$ (°)	0.403 (1)	0.396 (1)	0.387 (1)	0.378 (1)	0.367 (2)
$BV_{Na/K-O}$	1.03	1.02	1.02	1.01	1.01
BV_{Nb-O}	4.67	4.68	4.68	4.69	4.70

over the whole temperature range, which means that the upper face of the octahedron is larger than the lower face. Considering the cation displacements are all positive, this shows that the Nb atoms tend to move towards the upper large face, and so this result for the octahedral distortion is self-consistent. However, the *d* value does not show a well defined change with temperature despite the change in Nb displacements.

The same situation happens with the octahedral strain $(1 + \zeta = \cos\omega[c_H/a_H(6)^{1/2}])$, which describes elongation or compression of the octahedron along the triad axis. The value of ζ is negative, which indicates that the octahedra are compressed. But again no clear change of the strain over temperature is observed (Table 2). The connection between strain, tilt angle and rhombohedral angle was originally investigated by Thomas (1996). According to this, the octahedral strain $\eta = 1 + \zeta$ is a sum effect of the elongation related to the positive lattice strain ($\alpha_{pc} < 90°$) and the flattening due to the tilt angle. As the temperature increases, the tilt angle decreases and the rhombohedral angle becomes closer to 90°, which are two opposite factors affecting the octahedral strain. As ζ is very close to zero, it is understandable that the strain does not have an obvious correlation with the change of temperature.

3.2. $K_{0.30}Na_{0.70}NbO_3$ for $100 \leq T \leq 180$ K

The structure of $K_{0.30}Na_{0.70}NbO_3$ at 100 K was determined in the rhombohedral phase, using the *R*3*c* structure of $K_{0.05}Na_{0.95}NbO_3$ as a starting model. From 100 to 160 K, the refinement results of the data show that the structure remains in a single rhombohedral phase. The structural parameters are given in Table 3.

The lattice parameters in the hexagonal cell and the cation displacements are shown in Figs. 2(*a*) and (*b*). Comparing these values with those of $K_{0.05}Na_{0.95}NbO_3$ at low tempera-

Table 4
Observed and calculated value of the lattice strain related to the tilt angle.

η	ω	$90^\circ - \alpha_{pc}$(obs)	$90^\circ - \alpha_{pc}$(cal)
(*a*) $Na_{0.95}K_{0.05}NbO_3$			
0.99655 (8)	11.62 (2)	0.6623 (6)	0.6625
0.99657 (8)	11.83 (2)	0.6927 (6)	0.6928
0.99654 (9)	12.03 (2)	0.7196 (6)	0.7197
0.99647 (7)	12.19 (2)	0.7406 (5)	0.7407
0.99648 (7)	12.27 (2)	0.7527 (5)	0.7529
(*b*) $Na_{0.70}K_{0.30}NbO_3$			
1.0042 (1)	5.87 (4)	0.367 (2)	0.3675
1.00363 (7)	6.38 (3)	0.378 (1)	0.3789
1.00340 (7)	6.64 (3)	0.387 (1)	0.3877
1.00333 (7)	6.78 (3)	0.396 (1)	0.3967
1.00322 (7)	6.94 (3)	0.403 (1)	0.4040

ture, the lattice parameters, a_H and c_H, increase as expected. The parameter t, which measures the displacements of Nb from the centre of the octahedron, is approximately constant, while the parameter s, which is the shift of Na/K from the ideal perovskite position, decreases as the concentration of potassium increases.

The lattice strain ($90 - \alpha_{pc}{}^\circ$), at different temperatures, is plotted in Fig. 2(*c*). With increasing temperature, the lattice strain decreases almost linearly, while the rhombohedral angle (α_{pc}) itself is much closer to 90° compared with the $K_{0.05}Na_{0.95}NbO_3$ data.

The tilt angle ω from 100 to 180 K is plotted in Fig. 2(*d*). The value of ω is much smaller than the tilt angle in $K_{0.05}Na_{0.95}NbO_3$. The cation displacements and lattice strain indicate that the rhombohedral structure approaches the ideal perovskite structure and becomes less polar with increasing potassium content.

For $K_{0.30}Na_{0.70}NbO_3$, d is negative, as it is for $K_{0.05}Na_{0.95}NbO_3$, but there is a gradual increase in the absolute value of d with temperature (Table 3).

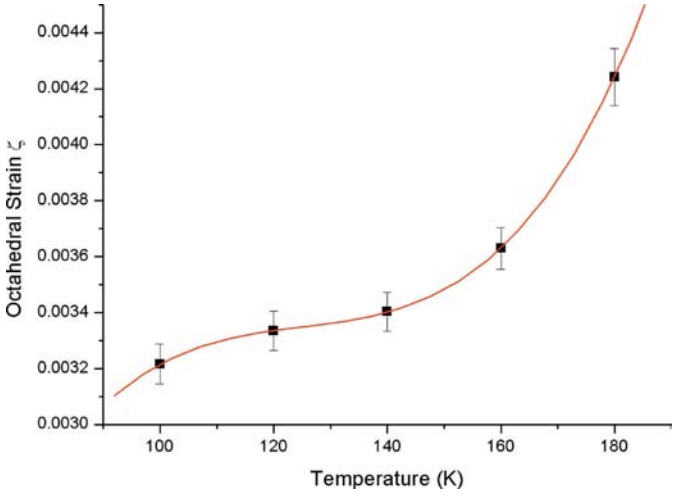

Figure 3
Octahedral strain (ζ) of $Na_{0.70}K_{0.30}NbO_3$ as a function of temperature.

Unlike at the lower-potassium end, the octahedral strain ζ of $K_{0.30}Na_{0.70}NbO_3$ is positive, which suggests that the octahedra are elongated. As discussed before, the tilt angle ω decreases markedly, and the flattening effect caused by the octahedral tilt is weaker. Thus, the elongation effect, caused by the lattice strain, is the major factor in this case and the octahedra change from being compressed to elongated. As the temperature increases, the value of ω drops from 6.94 (± 0.03) to 5.87 (±0.04)° (15.4%), while the value of the lattice strain drops from 0.403 (±0.001) to 0.367 (±0.002)° (8.9%). From a comparison with the $K_{0.05}Na_{0.95}NbO_3$ data, where ω drops from 12.27 (±0.02) to 11.62 (±0.02)° (5.3%) and the value of the lattice strain drops from 0.7527 (±0.0005) to 0.6623 (±0.0006) (12.0%), it is obvious that the lattice strain decreases much less for $K_{0.30}Na_{0.70}NbO_3$ and ω decreases more. Thus, the octahedra tend to be elongated more with increasing temperature and the value of ζ also increases. The same phenomenon of increasing lattice strain on approaching the MPB was observed in PZT, namely as the concentration of

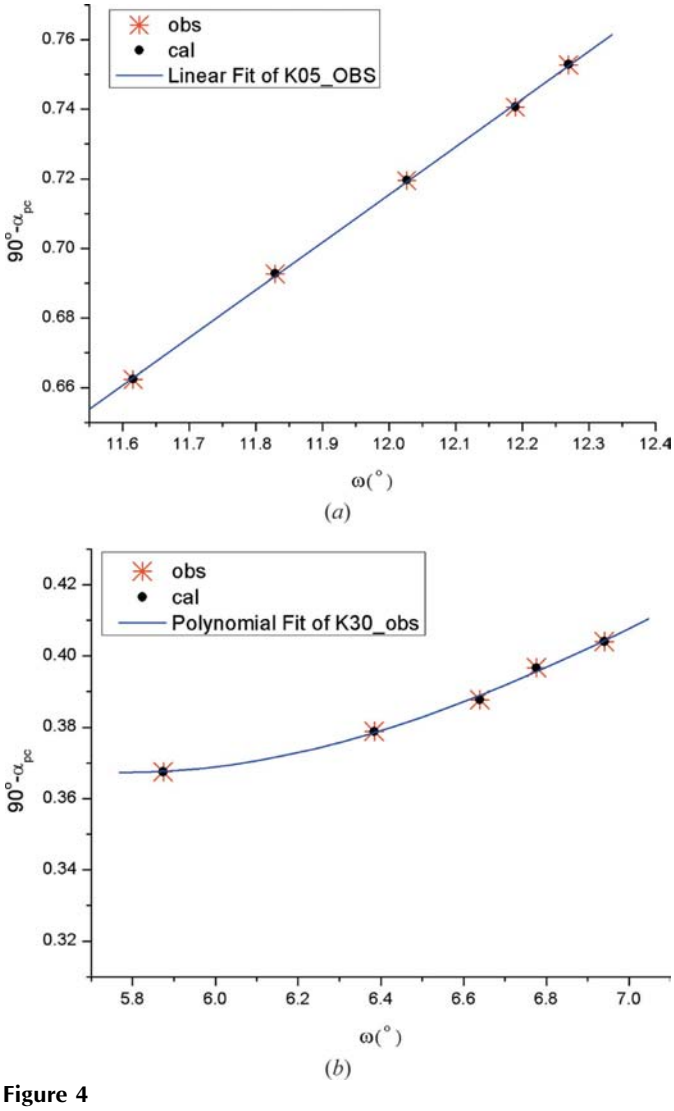

Figure 4
Tilt angle ω *versus* lattice strain $90 - \alpha_{pc}$. (*a*) $Na_{0.95}K_{0.05}NbO_3$ data; (*b*) $Na_{0.70}K_{0.30}NbO_3$ data.

Table 5
Structural parameters of $Na_{0.95}K_{0.05}NbO_3$ at room temperature and $Na_{0.70}K_{0.30}NbO_3$ at 200 K.

Radiation type	Neutron		
λ (Å)	1.60		
Detector	D2B		
Chemical formula	$Na_{0.95}K_{0.05}NbO_3$		$Na_{0.70}K_{0.30}NbO_3$
Temperature (K)	300		200
Phase type	Multiphase		Single phase
Crystal system	Monoclinic	Rhombohedral	Monoclinic
Space group	*Pm*	*R3c*	*Pm*
Tilt system	$a^-b^+c^-$	$a^-a^-a^-$	$a^0b^+c^0$
a (Å)	5.6012 (1)	5.5298 (3)	5.6587 (1)
b (Å)	7.7983 (2)	5.5298 (3)	3.93856 (5)
c (Å)	5.5480 (1)	13.769 (1)	5.6248 (1)
β (°)	90.051 (4)		90.073 (2)
$BV_{Na/K-O}$	0.95	1.05	1.02
BV_{Nb-O}	4.71	4.48	4.73
Relative proportion (%)	84	16	100
R_{wp}	0.0791 0.0599		0.0757
R_p			0.0583
GOF	2.98		2.02

Ti increases, the value of the lattice strain increases almost linearly. The change of ζ as a function of temperature for $K_{0.30}Na_{0.70}NbO_3$ is shown in Fig. 3.

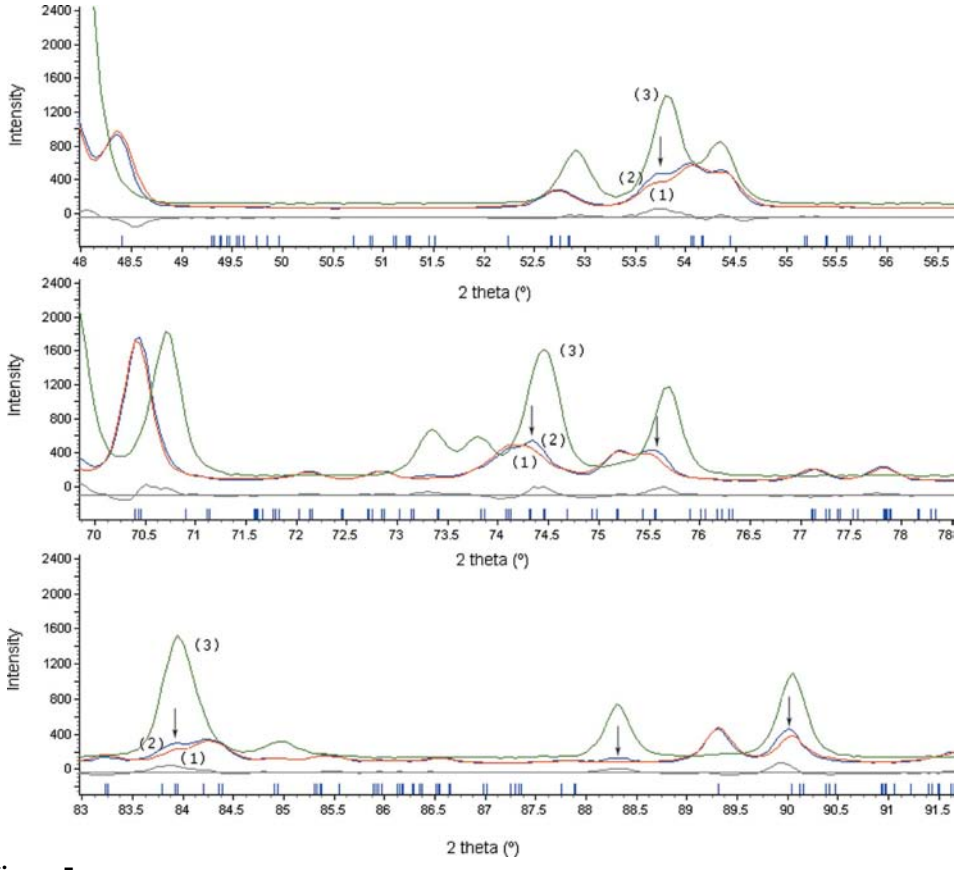

Figure 5
Observed and calculated neutron diffraction pattern (D2B, λ = 1.60 Å) at room temperature compared with the low-temperature powder profile. (1) Calculated pattern refined as a single monoclinic phase at room temperature (red); (2) observed pattern at room temperature (blue); (3) observed powder pattern in rhombohedral phase at 250 K (green). The arrows show the peaks that do not fit well in the red and blue patterns, while could be treated as the effect of the existence of the green one.

3.3. Discussion

The correlations between the tilt angle and the lattice strain for both samples are plotted in Fig. 4, and the curves are quite different from each other. According to Thomas (1996), when the value of the octahedral strains ($\eta = 1 + \zeta$) is between 0.95 and 1.05, the lattice strain can be expressed in terms of tilt angle as follows

$$90^\circ - \alpha_{pc} = \sum_{j=0}^{j=3} a_{0j}\eta^j + \sum_{i=1}^{4}\left(\sum_{j=0}^{3} a_{ij}\eta^j\right) < \omega >^i. \qquad (2)$$

In $K_{0.05}Na_{0.95}NbO_3$ and $K_{0.30}Na_{0.70}NbO_3$ the observed and calculated values are in remarkably good agreement (Table 4), showing that the structures are very well determined. In $K_{0.05}Na_{0.95}NbO_3$, ζ is negative and approximately constant, and so the value of ω increases almost linearly with increase of the lattice strain; while for $K_{0.30}Na_{0.70}NbO_3$ (ζ is positive and increases with temperature), a third-order polynomial correlation can be observed. Equation (2) predicts that when the range of the lattice strain value is very small and the η value is constant, the relationship between the tilt angle and the lattice strain is linear, as found for $K_{0.05}Na_{0.95}NbO_3$. However, when the η value is not constant, the relationship is not linear, as in $K_{0.30}Na_{0.70}NbO_3$. Thus, these two compounds represent two different regions of the application of (2).

4. Phase boundaries

4.1. Phases of $K_{0.05}Na_{0.95}NbO_3$ at 300 K

Neutron diffraction data taken at 300 K were initially refined as a single monoclinic phase with the space group *Pm* (phase *Q* according to Ahtee & Glazer, 1976). The tilt system of the NbO_6 octahedra was found to be $a^-b^+c^-$, and the *B*-cation displacement was in the positive direction between the *a* and *c* axes, which agrees with the theoretical approach by Stokes *et al.* (2002). The structure was refined in the true $(2)^{1/2}a_p \times 2b_p \times (2)^{1/2}c_p$ unit cell. In the refinement it was assumed that the octahedra are tilted as rigid units and therefore constraints were applied for the displacements (termed as *u*, *v*, *w*) of the O atoms as

$$u_{O6} = w_{O5};\ -w_{O6} = u_{O(5)}. \qquad (3)$$

Although most of the main peaks at low angles can be fitted using the monoclinic model, the observed fit was not satisfactory ($R_{wp} = 0.105$) and several peaks (especially at high angles) did not agree with the calculated profile very well (Fig. 5). The figure shows three high-angle parts of a single diffraction pattern fitted with the monoclinic model, with the observed low-temperature pattern added for comparison. All the unfitted peaks in the observed pattern have greater intensity than in the calculated patterns. Futhermore, for all the unfitted peaks there is a strong peak at the same position in the low-temperature rhombohedral pattern. Therefore, the unfitted peaks can be explained by the appearance of the rhombohedral peaks and it indicates that at 300 K the rhombohedral phase is already present. The coexistence of the two phases suggests a first-order phase transition boundary near room temperature.

The neutron data were refined again using a mixture of two phases, both monoclinic *Pm* and rhombohedral *R*3*c*, and the calculated profile fit was much better ($R_{wp} = 0.079$). The details of the structure are shown in Table 5, and the relative proportion was refined in *TOPAS Academic*.

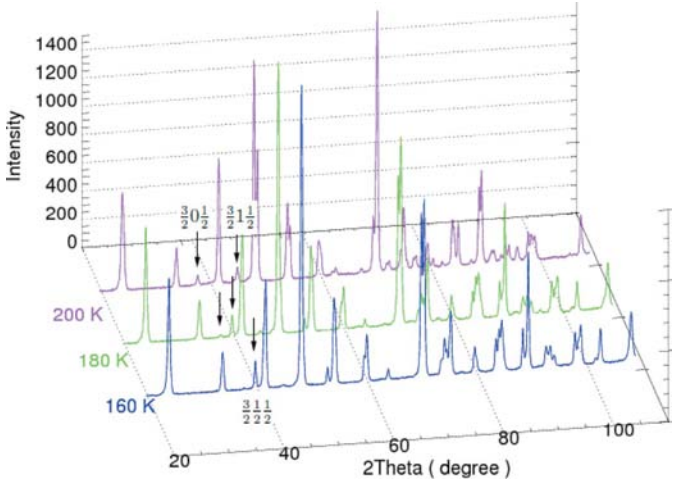

Figure 6
D2B neutron diffraction ($\lambda = 1.60$ Å) patterns of $Na_{0.70}K_{0.30}NbO_3$ at 160, 180 and 200 K. Arrows indicate the positions for the tilt peaks.

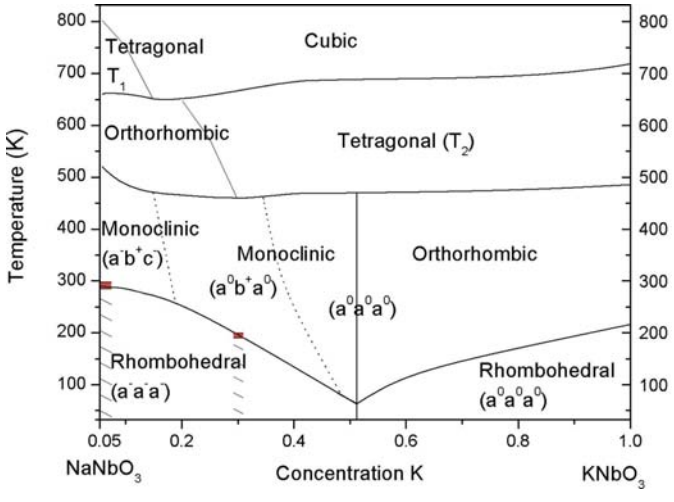

Figure 7
A revised phase diagram for KNN produced based on the study so far. The shading marks the regions described in this paper. The red lines show the rhombohedral-monoclinic phase boundaries: two-phase coexistence regions. The data regarding the tilt systems in the composition range of $x = 0.10$ to $x = 0.26$ will be published in more detail in a later paper (Baker *et al.*, 2009*b*).

4.2. Rhombohedral-monoclinic phase boundary of $K_{0.30}Na_{0.70}NbO_3$

It has been reported in Baker *et al.* (2009*a*) that the room-temperature structure of $K_{0.30}Na_{0.70}NbO_3$ is monoclinic, *Pm*, with the $a^0b^+c^0$ tilt, which has the same space group as $K_{0.05}Na_{0.95}NbO_3$ but a different tilt system. As the potassium concentration increases to between 15 and 20%, the KNN structure transforms by losing the two minus tilts to change from $a^-b^+c^-$ to $a^0b^+c^0$. The data collected at 200 K were refined initially using the same phase in the true cell $(2)^{1/2}a_p \times b_p \times (2)^{1/2}c_p$. The structural results are shown in Table 5.[1] The good fit confirms that $K_{0.30}Na_{0.70}NbO_3$ is in this single phase from room temperature to ~ 200 K.

A coexistence of the rhombohedral and monoclinic phases was observed at 180 K: in the diffraction pattern this was indicated by the plus tilt peaks appearing while the minus tilt peaks had not disappeared completely. The temperature is therefore close to the phase boundary between the low-temperature phase *R*3*c* and the room-temperature phase *Pm*. The diffraction patterns at 160, 180 and 200 K are shown in Fig. 6.

5. Conclusions

The low-temperature $K_xNa_{1-x}NbO_3$ ($x = 0.05$, $x = 0.30$) structures have been shown for the first time to have rhombohedral symmetry, space group *R*3*c*, with the tilt system $a^-a^-a^-$. Geometrical structural parameters were studied and it was found that with the increase of the potassium concentration, the NbO_6 octahedral strain changes from compression to elongation. The octahedral strain of $K_{0.30}Na_{0.70}NbO_3$ increases when the material approaches the rhombohedral-monoclinic phase boundary, which is similar to the behavior of PZT on approaching the MPB.

A coexistence of rhombohedral and monoclinic phases was observed at 300 K for $K_{0.05}Na_{0.95}NbO_3$, which indicates a first-order phase boundary. The same phenomenon was found around 180 K for $K_{0.30}Na_{0.70}NbO_3$.

A phase diagram of KNN produced based on the results so far is shown in Fig. 7. The dashed lines indicate the phase boundaries that are still under investigation as part of this study.

[1] Supplementary data for this paper are available from the IUCr electronic archives (Reference: WF5039). Services for accessing these data are described at the back of the journal.

The authors would like to thank the Institut Max von Laue–Paul Langevin (ILL), Grenoble, France, for allowing the neutron diffraction experiments to be carried out and the support of the technical staff there. N. Zhang is also grateful for the financial support from the Clarendon Fund, Oxford, and D. Baker for support from the Engineering and Physical Sciences Research Council.

References

Ahtee, M. & Glazer, A. M. (1976). *Acta Cryst.* A**32**, 434–446.
Ahtee, M. & Hewat, A. W. (1975). *Acta Cryst.* A**31**, 846–850.
Ahtee, M. & Hewat, A. W. (1978). *Acta Cryst.* A**34**, 309–317.
Baker, D. W., Thomas, P. A., Zhang, N. & Glazer, A. M. (2009*a*). *Acta Cryst.* B**65**, 22–28.
Baker, D. W., Thomas, P. A., Zhang, N. & Glazer, A. M. (2009*b*). In preparation.
Brown, I. D. (1981). *Structure and Bonding*, Vol. 2. Berlin: Springer-Verlag.
Coelho, A. A. (2005). *J. Appl. Cryst.* **38**, 455–461.
Darlington, C. N. W. & Megaw, H. D. (1973). *Acta Cryst.* B**29**, 2171–2185.
Glazer, A. M. (1972). *Acta Cryst.* B**28**, 3384–3392.
Glazer, A. M., Thomas, P. A., Baba-Kishi, K. Z., Pang, G. K. H. & Tai, C. W. (2004). *Phys. Rev. B*, **70**, 184123.
Hewat, A. W. (1973). *J. Phys. C Solid State Phys.* **6**, 2559–2572.
Hewat, A. W. (1979). *Acta Cryst.* A**35**, 248.
Megaw, H. D. & Darlington, C. N. W. (1975). *Acta Cryst.* A**31**, 161–173.
Mishra, S. K., Choudhury, N., Chaplot, S. L., Krishna, P. S. R. & Mittal, R. (2007). *Phys. Rev. B*, **76**, 024110.
Saito, Y., Takao, H., Tani, T., Nonoyama, T., Takatori, K., Homma, T., Nagaya, T. & Nakamura, M. (2004). *Nature*, **432**, 84–87.
Stokes, H. T., Kisi, E. H., Hatch, D. M. & Howard, C. J. (2002). *Acta Cryst.* B**58**, 934–938.
Thomas, N. W. (1996). *Acta Cryst.* B**52**, 954–960.